RNA (2002), *8*:464–477. Cambridge University Press. Printed in the USA.

DOI: 10.1017.S1355838202020289

Delta ribozyme benefits from a good stability in vitro that becomes outstanding in vivo

DOMINIQUE LÉVESQUE,[1] SANAA CHOUFANI,[2] and JEAN-PIERRE PERREAULT[1]

[1]Département de biochimie, Université de Sherbrooke, Sherbrooke, Québec, J1H 5N4, Canada
[2]Département d'anatomie et biologie cellulaire, Université de Sherbrooke, Sherbrooke, Québec, J1H 5N4, Canada

ABSTRACT

The stability of a *trans*-acting *delta* ribozyme was studied under various conditions. Although in vitro (i.e., in the presence of protein extracts) this *delta* ribozyme appears to be only slightly more stable than a hammerhead ribozyme, in vivo (i.e., after cell transfection) it exhibits an outstanding stability that manifests itself in the calculated half-life of over 100 h regardless of the means of transfection. The P2 stem, which includes both the 5′ and 3′ ends, is shown to play a critical role in this stability. Direct mutagenesis of the most nuclease susceptible nucleotides failed to generate a more stable ribozyme that retained the same catalytic potential. Clearly, *delta* ribozyme appears to be well adapted to the human cell environment, and is therefore ideal for the development of a gene-inactivation system.

Keywords: gene therapy; molecular evolution; ribozyme; RNA stability; RNA structure–function

INTRODUCTION

The ability of ribozymes to specifically recognize a substrate and subsequently catalyze its cleavage makes them attractive as therapeutic tools for the inactivation of both viral RNAs and the mRNAs associated with various diseases (for review, see Rossi, 2000). However, several problems remain to be solved before we generate a useful gene-inactivation system based on catalytic RNA. The cellular stability of ribozymes is one of the most important limiting factors. To prevent fast degradation by the host cellular nucleases, it is possible to prepare chemically stabilized ribozymes through the use of both modified phosphates and 2′-hydroxyl groups (Verma & Eckstein, 1998). Unfortunately, in addition to being expensive, this type of synthetic approach generates other problems that must be overcome, such as the stability of the synthetic ribozymes in serum and the necessity of providing sufficient numbers of molecules into specific cells. To avoid many of these difficulties, the endogenous synthesis of ribozymes appears to be a preferable approach to ribozyme-based therapy, and should permit the utilization of the many drug delivery systems that are currently under development for various gene-therapy approaches.

Reprint requests to: Jean-Pierre Perreault, Département de biochimie, Université de Sherbrooke, Sherbrooke, Québec, J1H 5N4, Canada; e-mail: jperre01@courrier.usherb.ca.

Both genomic and antigenomic hepatitis *delta* virus (HDV) RNAs have self-cleavage activities that produce 2′,3′-cyclic phosphate and 5′-hydroxyl termini (for reviews, see Been & Wickham, 1997; Doherty & Doudna, 2000). A model secondary structure, which is well supported by experimental data, has been proposed for the self-cleaving *delta* sequence. This structure consists of one stem (P1), one pseudoknot (P2), two stem-loops (P3 and P4), and three single-stranded regions (J1/2, J1/4, and J4/2; Fig. 1). An additional pseudoknot, named P1.1, that is formed by 2 GC bp between nucleotides of the J1/4 junction and the P3 loop, has also been reported (Ferré-D'Amaré et al., 1998; Wadkins et al., 1999). *Trans*-acting ribozymes have been developed by removing the J1/2 junction, thereby producing one molecule possessing the substrate sequence and the other the catalytic site. *Delta* self-catalytic RNA has been used in cells to release a hammerhead ribozyme that subsequently acted in *trans* on a herpes simplex virus mRNA, as well as for the synthesis of RNA with the precise termini required in the production of defective interfering particles of vesicular stomatitis virus (Pattnaik et al., 1992; Chowrira et al., 1994). The specific cleavage in vitro of the mRNA encoding the *delta* antigen (HDAg) in *trans* by *delta* ribozymes has been reported, showing their potential for the further development of a system for inhibiting gene expression (Roy et al., 1999). This potential for cleavage in *trans* was subsequently demonstrated in vivo using another RNA target (Kato et al., 2001).

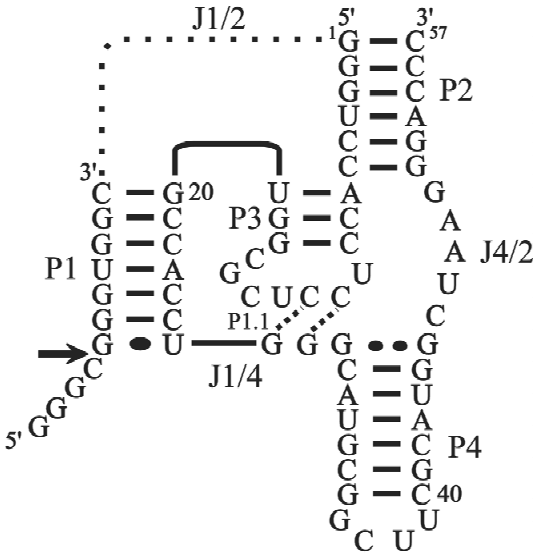

FIGURE 1. Secondary structure and sequence of the antigenomic *trans*-acting *delta* Rz-12. Paired regions are numbered P1, P1.1 (dotted lines), P2, P3, and P4, and joining regions are named according to the paired elements they link. A dashed line represents the sequence removed from the self-cleaving RNA strand (J1/2 region) so as to generate the *trans*-acting ribozyme. The arrow indicates the substrate cleavage site. The homopurine base pair at the top of the P4 stem is represented by two dots (G••G), and the wobble base pair by one (G•U).

Delta ribozyme possesses several unique features, all of which are related to the fact that it is the only catalytic RNA motif that has been discovered in humans. Thus, we postulate that *delta* self-cleaving ribozymes have evolved so as to possess optimal activity in this cellular environment. For example, *delta* ribozyme functions naturally at low magnesium concentrations (~1 mM), and is the only ribozyme known to be fully active in the presence of calcium (Doherty & Doudna, 2000). This contrasts with all other ribozymes that are currently attracting interest as tools for gene inactivation as these are all derived from RNA species retrieved from nonmammalian cells. For example, the hammerhead ribozyme is derived from plant viroids, which may explain its relative instability in human cells (Sioud et al., 1994; Gagnon & Rossi, 2000). Before investing time in the development of *delta* ribozyme as a therapeutic gene-inactivation tool, we considered it prudent to investigate whether or not its evolution as part of HDV in human cells gives it any benefits in this regard.

RESULTS

In vitro stability of *delta* ribozyme

Among the collection of *delta* ribozymes that exhibit *trans* catalytic cleavage of the HDAg mRNA, Rz-12 was found to be the most active (Roy et al., 1999); hence, it was used as a model ribozyme in this study (Fig. 1). A trace amount of ^{32}P-5′-end-labeled Rz-12 was incubated at 37 °C in the presence of a total protein extract isolated from HepG2 cells, a cell line which originates from a human hepatocarcinoma and is frequently used to study hepatitis viruses. Aliquots were removed from the reaction at various time points and analyzed by electrophoresis through denaturing 10% polyacrylamide gels (PAGE). A typical autoradiogram is shown in Figure 2A. The hydrolysis increases with the time of incubation, and appears to be specific for certain phosphodiester bonds. Various modifications of the protocol were tested to characterize the assay (data not shown). First, the level of hydrolysis was shown to vary proportionally with the concentration of protein extract (i.e., 0.1–4 μg). With a high concentration of protein extract, all radioactivity was found at the bottom of the gel, indicating that no ribozyme was trapped in a nuclease-resistant conformation. Second, the hydrolysis was shown to have no magnesium requirement, as is illustrated by the fact that the fraction of intact ribozyme at any given time was smaller in the presence of EDTA. Third, similar hydrolytic patterns were obtained when using protein extracts isolated from two other unrelated cell lines (OST7 and HEK 293 cells). The OST7 cell line originates from a murine fibroblast, and HEK 293 is derived from a human embryonic kidney cell line transformed with an adenovirus. Clearly, the results described below are not specific to the HepG2 protein extract.

Maps of the phosphodiester bonds most susceptible to nuclease attack by the HepG2 protein extract were determined for several versions of the *delta* ribozyme (Fig. 2). Varying exposures of the gel were required to reveal all of the bands. The most susceptible phosphodiester bonds of Rz-12 were those at positions U_{10}, U_{13}, and C_{14} of the L3 loop, C_{22}, C_{25}, and U_{26} of the P1 region, C_{30} at the top of the P4 stem-loop, and A_{49} in the J4/2 junction (note that the bonds were numbered by considering the 5′-end phosphate as number 1). In the gel shown in Figure 2A, the shorter products comigrated with the dye front (BPB). Electrophoresis through a 20% PAGE gel eliminated this problem, and revealed that the shorter products were mainly free ^{32}P-NMP (data not shown). A single point mutation of C_{47} for A_{47}, which produces an inactive version of the ribozyme (i.e., Rz-12C47A), does not alter the hydrolysis pattern (Fig. 2B). Ribozymes Rz-1, Rz-6, and Rz-11, which originate from the collection tested for the ability to cleave the HDAg mRNA (Roy et al., 1999), yielded hydrolytic patterns almost identical to that for Rz-12 (Fig. 2C–E). The differences were limited to the following: (1) The phosphodiester bond at position U_{10} was hydrolyzed in all ribozymes, although at different levels; (2) Rz-6 and Rz-12 are hydrolyzed at C_{30}, whereas Rz-1 and Rz-11 are not, instead showing bond cleavage at positions G_{45} and G_{46}; and (3) there is an

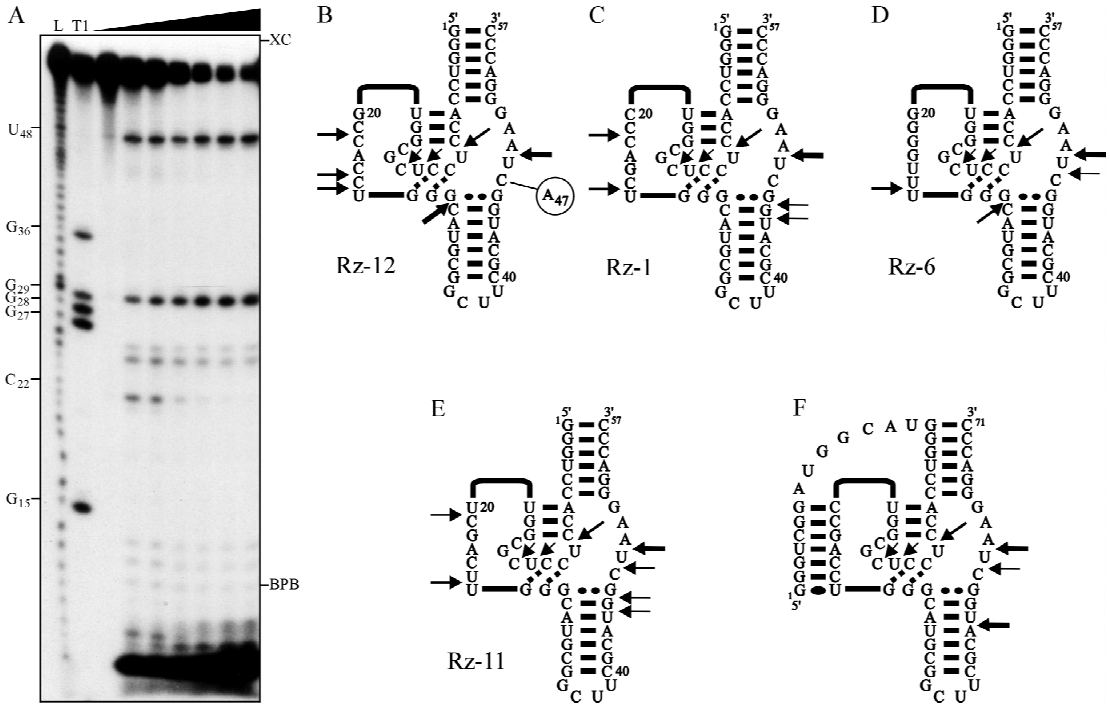

FIGURE 2. In vitro hydrolysis of various versions of *delta* ribozyme. **A:** Typical autoradiogram of a denaturing 10% PAGE gel of 5′-end-labeled Rz-12 incubated with a protein extract isolated from HepG2 cells. The first and second lanes are ladders formed by alkaline (L) and ribonuclease T1 (T1) hydrolysis, respectively. Lanes 3 to 9 are hydrolysis patterns of Rz-12 resulting from increasing incubation times (0, 10, 20, 60, 120, 180, and 240 min). The migrational positions of xylene cyanol (XC) and bromophenol blue (BPB) are indicated. **B–F:** Schematic representations of the hydrolysis patterns obtained with various *trans*-acting ribozymes (**B** to **E**) and a *cis*-acting version (**F**). The arrows indicate the phosphodiester bonds hydrolyzed, with the wider ones indicating the most susceptible positions. The encircled A_{47} in **B** illustrates an inactive mutant of Rz-12 (Rz-12C47A) that was tested.

additional cleaved phosphodiester bond at position U_{48} in both Rz-6 and Rz-11. These nuclease mapping modifications most likely reveal discrete structural differences between the ribozymes. The most important modifications between these ribozymes occur within the single-stranded P1 region, which is different in each ribozyme. To mimic a ribozyme–substrate complex, a self-cleaved *cis*-acting *delta* ribozyme (i.e., the reaction product) was incubated under the same conditions (Fig. 2F). The phosphodiester bonds hydrolyzed were limited to those at positions U_{10}, C_{13}, U_{14}, U_{44}, U_{48}, and A_{49}. No phosphodiester bonds of the P1 region were hydrolyzed, indicating that the folding into a double-stranded region was enough to stabilize this domain.

With the exception of the cleaved phosphodiester bonds at the top of the P4 stem, the most susceptible linkages were found in single-stranded regions (i.e., P1, L3, and the J4/2 domains). More specifically, these hydrolyses occurred at phosphodiester bonds composed of cytosine–uridine (U_{10}, U_{13}, and U_{48}), uridine–cytosine (C_{14}) and uridine–adenine (A_{49}) linkages, an observation that correlates with the predominance of endoribonucleases specific for phosphodiester bonds between pyrimidines or for uridine–adenine linkages in single-stranded regions of RNA (for a review, see Sorrentino, 1998).

In vitro decay of *delta* ribozymes as compared to other RNA species

To learn more about the in vitro stability of Rz-12, kinetic analysis of the hydrolysis was performed, and the data compared to that of various RNA species. Radiolabeled RNA was incubated in the presence of HepG2 protein extracts, and aliquots removed at various time points. These were then subjected to PAGE fractionation, and the fraction of intact ribozyme evaluated by phosphorimaging (Fig. 3). Plotting of the fraction of intact Rz-12 as a function of time revealed a biphasic relationship. The half-lives ($t_{1/2}$) for each portion of the curves were determined as described previously for hammerhead ribozymes (Sioud et al., 1994; see Table 1). The first portion of the curve corresponds to a fast decay, and the second portion to a slow decay (i.e., that over 60 min). At long times ($t > 120$ min), when the fast decay component had died away and only the slow decay remained, a curve was found to fit the data. When this curve was substracted from the experimental data, the resulting values clustered around zero at long times. The slow degradation phase has an estimated $t_{1/2}$ of 44 h. However, at short times ($t < 1$ h) these residual differences deviated systematically from zero and described the fast decay component. An ex-

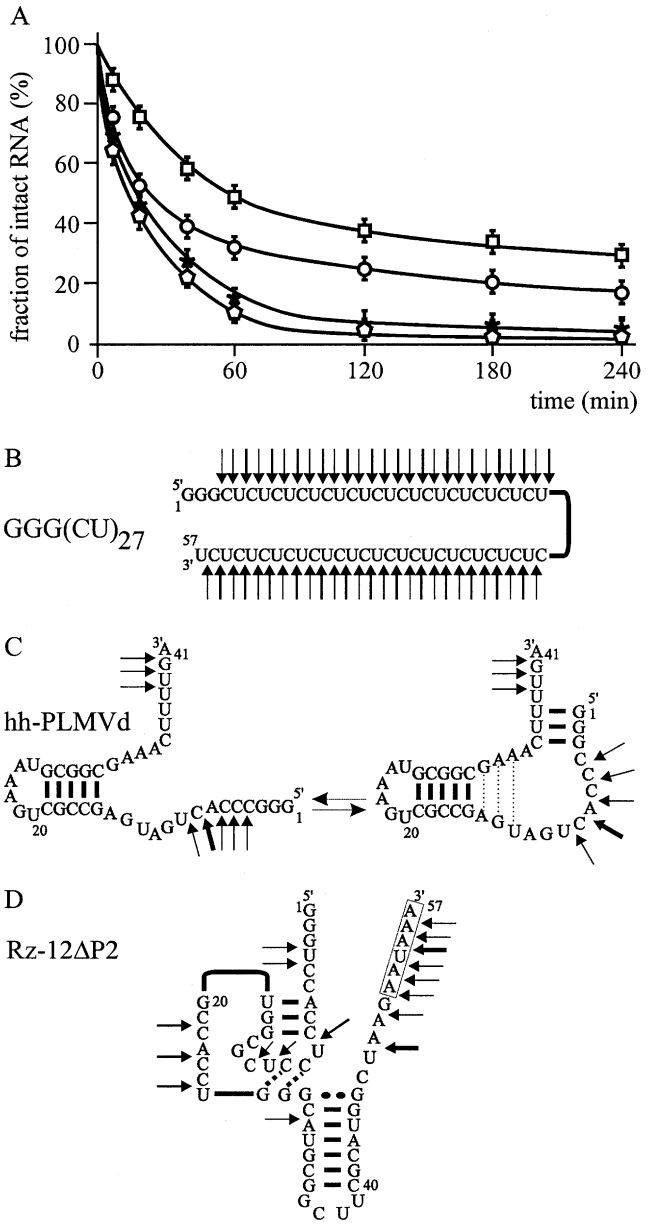

FIGURE 3. In vitro decay and degradation patterns of various RNA species. **A:** Plot of the fraction of intact RNA species as a function of time for Rz-12 (squares), hammerhead ribozyme (hh-PLMVd; circles), Rz-12ΔP2 (stars), and GGG(CU)$_{27}$ (pentagons). **B**–**D:** Nucleotide sequences, proposed secondary structures, and degradation patterns of these RNA species. The arrows indicate the phosphodiester bonds hydrolyzed, with the wider ones indicating the most susceptible positions. For the hammerhead ribozyme, an alternative structure including a greater number of base pairs is also shown.

ponential curve was also fitted to the fast decay data, and yielded an estimated $t_{1/2}$ of 1.3 h. Other versions of *delta* ribozyme, such as Rz-1 and Rz-11, had virtually identical $t_{1/2}$.

Two RNA controls were tested. First, a molecule of 57 nt composed of three guanosines followed by 27 repetitions of the dinucleotide CU (i.e., GGG(CU)$_{27}$) gave data that was fit by a simple exponential with a $t_{1/2}$ of 12 min (Fig. 3A; Table 1). The products of hydrolysis

TABLE 1. Half-life times (hours) of various RNA species.

			In vivo	
Species	Decay	In vitro	Lipofection	Electroporation
Rz-12	fast	1.3 ± 0.3	—	—
	slow	44 ± 3	120 ± 8	100 ± 9
Rz-U48A	slow	n.d.	160 ± 5	n.d.
Hammerhead	fast	40 ± 6*	12 ± 2	11.3 ± 3.1
	slow	29 ± 2	45 ± 2	49 ± 6
GGG(CU)$_{27}$	fast	12 ± 2*	4.2 ± 1.7	n.d.
Rz-12ΔP2	fast	22 ± 2*	6.8 ± 1.1	10.4 ± 2.7

*:Half-life times in minutes rather than in hours.
—: No fast decay observed.
n.d.: Not determined.

formed a ladder on the gels, indicating that this is a single-stranded RNA species (Fig. 3B). Second, we analyzed a *trans*-acting hammerhead ribozyme derived from the *cis*-acting motif of the peach latent mosaic viroid strand of minus polarity (Fig. 3C; Beaudry et al., 1995). The hydrolysis pattern of this hammerhead ribozyme is shown by the arrows in Figure 3C. The secondary structure on the right, which includes an additional 3-bp stem, appeared to better fit the observed hydrolysis pattern than the predicted one (on the left). The plot of the fraction of intact ribozyme as a function of time was fit by a biphasic relation for which the fast and slow decays had $t_{1/2}$ of 40 min and 29.3 h, respectively. Although this might be an overestimation if the additional stem contributes to stabilizing this RNA species, comparing these $t_{1/2}$ with those of Rz-12 shows that the *delta* ribozyme is at least twofold more stable in vitro.

The stability of the *delta* ribozyme might be caused by the fact that both the 5′ and 3′ ends are located in the double-stranded region that forms the P2 stem, thereby limiting access of the single-stranded exonucleases. When a mutant with a disrupted P2 stem was examined (Fig. 3D, Rz-12ΔP2), all phosphodiester bonds in the 3′-end region, and two in the 5′-end region, were strongly hydrolyzed as compared to Rz-12. Clearly, single-stranded exonucleases hydrolyze both ends of the mutant. Although it is not clear which secondary structure was adopted by Rz-12ΔP2, it had a rapid decay fitted by a simple exponential with a $t_{1/2}$ of only 22 min (Fig. 3A). This is a fivefold faster decay than the original Rz-12, indicating that the P2 stem plays a critical role in the stability of *delta* ribozyme.

Attempt to increase the stability of *delta* ribozyme

Regardless of the version of the *delta* ribozyme used, only five single-stranded phosphodiester bonds were

demonstrated to be consistently hydrolyzed by cellular nucleases (i.e., U_{10}, U_{13}, C_{14}, U_{48}, and A_{49}). Although U_{10} cannot be altered to increase the stability of the ribozyme because it has been shown to be crucial to the catalytic activity of the ribozyme (Been & Wickham, 1997), the other four positions may tolerate base substitutions without necessarily reducing the catalytic activity. To choose which nucleotide should be used to replace these 4 nt, two points need to be considered. First, as single-stranded pyrimidines are more susceptible to hydrolysis than purines, guanines or adenines were included at those positions. Second, the compilation of natural variants of the antigenomic *delta* self-cleaving motifs, which includes 23 sequences (Lafontaine et al., 1997), shows: (1) position 48 is occupied by either an adenine, a cytosine, or an uridine; therefore mutant U48A was favored; (2) two sequences had a G_{49} instead of the A_{49}; therefore, mutant A49G was tested; and (3) perfect conservation of positions U_{13} and C_{14} is observed among all variants; hence it was arbitrarily decided to prepare the mutants U13G and C14A. The cloning strategy was based on the use of a DNA oligonucleotide coding for the ribozyme sequence that was partially randomized at these positions in order to offer both the version with the original nucleotides and the one with the mutated bases at each position (Fig. 4A). This strategy offers the advantage of recovering versions including more than one mutation.

The cleavage activity for all mutants was determined using a small model substrate of 11 nt under single-turnover conditions. Trace amounts of ^{32}P-5′-labeled substrate ($<$1 nM), which produces RNA products of 4 and 7 nt, were incubated in the presence of an excess of ribozyme (200 nM). Typical results are shown in Figure 4B,C. Rate constants (k_{obs}) and the maximal cleavage percentage (i.e., the end point) were determined (Table 2). For the single-mutation ribozymes, the catalytic activity varied depending on the base identity at each position. The mutant U13G had a k_{obs} of 0.17 min^{-1}, which is slightly lower than the 0.22 min^{-1} observed with the original Rz-12 (i.e., also named wild-type, WT). The maximal cleavage percentage was more significantly affected, decreasing from 64% for Rz-12 to 30% for the mutant. The insertion of an adenosine at position 14 (i.e., mutant C14A) drastically decreased the k_{obs} by 10-fold to 0.023 min^{-1}, and the maximal cleavage percentage decreased to 27%. In contrast, the mutant U48A had a k_{obs} and a maximal cleavage percentage that increased to 0.25 min^{-1} and 74%, respectively. Finally, the mutant A49G showed a three-fold decrease in the k_{obs} to 0.080 min^{-1}, and the maximal cleavage percentage decreased to 45%. When more than 1 nt was altered, both the k_{obs} and maximal cleavage percentage decreased significantly.

To accurately assess the effect of the single mutations, kinetic analyses were performed under pre-steady-state conditions. Pseudo-first-order cleavage rate constants (k_2 and K'_M) were measured with an excess of ribozyme (Table 2). In summary, although the mutant U48A gave a slightly more active ribozyme, the decrease in the cleavage activity was more significant when passing from mutant U13G to A49G and finally to C14A. The variations in the kinetic parameters differed for each mutant according to the effect of the mutation on the reaction mechanism. For example, the U13G mutant has a k_2 similar to that of the original Rz-12, whereas its K'_M was slightly increased (i.e., 25.3 nM compared to 16.8). As position 13 is located in the L3 loop, and not in the P1 stem region responsible for the substrate binding, it appears reasonable to suggest that the increase in K'_M reflects a slower formation of the active ribozyme–substrate (RzS) complex. After binding of the substrate to the ribozyme, a conformational rearrangement has to occur to produce the active RzS complex (Mercure et al., 1998). It has been proposed that the formation of the P1.1 pseudoknot, which involves formation of the base pairs $C_{11}C_{12}$-$G_{27}G_{28}$, is crucial in this structural transition (Nishikawa & Nishikawa, 2000). One possibility is that an adjacent purine, possibly G_{13}, limits the structural rearrangement. As a consequence, the adoption of the active RzS complex is limited, and the K'_M is increased. The kinetic parameters were estimated for the double mutant U13G-U48A to see whether or not the presence of A_{48} preserves the activity in the presence of G_{13}. This double mutant had an slightly lower overall activity than the single mutant (U13G), revealing that the presence of A_{48} did not compensate, even partially, for the activity lost due the presence of a guanine residue at position 13. Clearly, the 2 nt mutated in the J4/2 junction showed less constraints than those in the L3 loop. These data are in good agreement with the sequence conservation of the natural variants where the nucleotides within L3 are highly conserved and cannot be substituted without drastically affecting the activity, whereas those of the J4/2 region show some flexibility.

The stability of the mutants was verified by incubation in the presence of HepG2 protein extracts as described above. Figure 4D shows an autoradiogram of a comparative analysis of nine *delta* ribozymes incubated for 20 min. In general, inclusion of a single mutation results in the stabilization of the adjacent phosphodiester bonds. The counterbalance to this is that at least one other bond is more susceptible to the activity of the nucleases. For example, the presence of G_{13} stabilized the phosphodiester bonds at positions 13 and 14, but that at position 22 was hydrolyzed several-fold more than in the original Rz-12 (compare lines WT+ and U13G). Similarly, when a mutation was performed within the J4/2 region, the phosphodiester bonds at position 26 and 30 were at least 10 times more susceptible to nuclease activity (compare U48A to U13G-U48A-A49G). Similarly, the C14A mutation enhances the hydrolysis at positions A_{14} and U_{44}. The fact that no

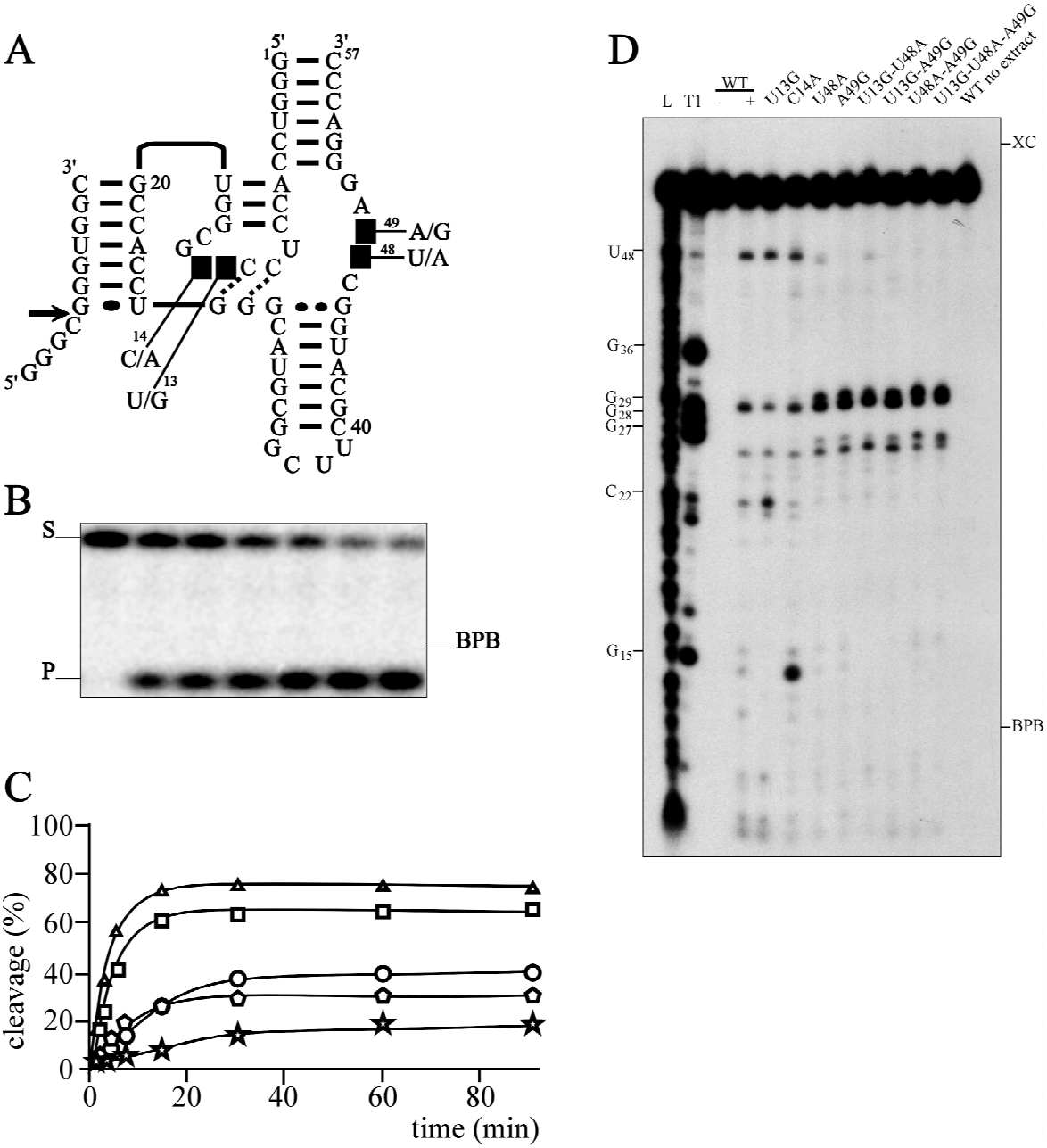

FIGURE 4. Activity and degradation patterns of several Rz-12 mutants. **A:** Schematic representation of the mutational strategy adopted with Rz-12. The secondary structure is shown in accordance with Figure 1. **B:** Example of a denaturing 20% PAGE autoradiogram of a cleavage assay. Left to right are aliquots removed from the reaction mixture after 0, 2, 5, 10, 20, 40, and 60 min. S, P, and BPB represent the substrate, product, and bromophenol blue, respectively. **C:** Graphical representation of the kinetic analyses of the single mutants derived from Rz-12. Experimental data were plotted as a function of time for Rz-12 (squares), U48A (triangles), A49G (circles), U13G (pentagons), and C14A (stars). **D:** Autoradiogram of a denaturing 10% PAGE of the degradation pattern of various Rz-12 mutants. The mutants are identified on the top of the gel. 5′-end-labeled mutants (500 ng) were incubated for 20 min in the presence of a HepG2 protein extract (500 ng). WT indicates the Rz-12 sequence, and (−) and (+) indicate times 0 and 20 min, respectively. The first and second lanes are ladders formed by alkaline (L) and ribonuclease T1 (T1) hydrolysis, respectively.

mutation improved the stability of *delta* ribozyme receives additional support from studies of stability versus the time (data not shown). The percentage of intact ribozymes decreased more rapidly for most mutants as compared to the original Rz-12. Clearly the original sequence, which is largely based on the wild-type, remains the best tested ribozyme in terms of both the catalytic potential and the in vitro stability.

TABLE 2. Kinetic parameters of various mutants of Rz-12.

Rz mutant	k_{obs} (min^{-1})	Maximal cleavage (%)	k_2 (min^{-1})	K'_M (nM)	k_2/K'_M (min^{-1} M^{-1})
WT	0.22	64	0.21 ± 0.03	16.8 ± 1.9	1.25×10^7
U13G	0.17	30	0.19 ± 0.03	25.3 ± 3.6	7.5×10^6
C14A	0.023	27	0.024 ± 0.010	19.7 ± 4.7	1.2×10^6
U48A	0.25	74	0.23 ± 0.02	11.8 ± 1.4	1.9×10^7
A49G	0.080	45	0.082 ± 0.010	20.4 ± 3.1	5.1×10^6
U13G-C14A	0.013	16			
U13G-U48A	0.088	29	0.10 ± 0.03	16.1 ± 4.9	6.2×10^6
U13G-A49G	0.031	18			
C14A-U48A	0.025	20			
C14A-A49G	0.015	8.0			
U48A-A49G	0.021	19			
U13G-C14A-U48A	0.026	9.0			
U13G-C14A-A49G	n.d.	<5			
U13G-U48A-A49G	0.016	7.5			
C14A-U48A-A49G	n.d.	<5			
U13G-C14A-U48A-A49G	n.d.	<5			

n.d.: Not determined.

Cellular uptake and in vivo stability of *delta* ribozyme

To evaluate the biological relevance of the previous data, a series of in vivo experiments were performed. Labeled (^{32}P) Rz-12 (100 ng) was transfected into HepG2 cells at 80% confluence using either Lipofectamine (Gibco-BRL) or Effectene (Qiagen). In the absence of liposome reagent, only trace amounts of radioactive ribozyme were recovered from the cells. Two hours posttransfection, an average of 60% of the ^{32}P-labeled ribozyme molecules was found within the cells, regardless of the transfection reagent used. Similar efficiencies of cellular uptake were observed after washing the cells several times with either a phosphate (pH 7.4) or a glycine (pH 2.8) buffer to remove all extracellular traces of the ribozyme. The efficiencies of cellular uptake were observed to be unaffected by the cell line used (e.g., HepG2 or OST7), the particular version of *delta* ribozyme, and the concentration of the RNA (0.1 to 2.5 μg). Finally, the integrity of the RNA recovered after the manipulation was verified by both agarose gel electrophoresis, so as to visualize both the rRNA and the tRNA, and polyacrylamide gel electrophoresis, so as to visualize the small radioactive RNA species studied (see below). Thus, the use of liposome reagents is an efficient means of inducing the cellular uptake of *delta* ribozyme. Based on the amount of ribozyme and the number of cells used for the transfections, we estimated that about 1–2 $\times$ 10^7 copies of *delta* ribozyme were incorporated per cell. This result is in agreement with previous reports based on the uptake of other small nucleic acid molecules (Kariko et al., 1994; Prasmickaite et al., 1998).

Following the efficient transfection of 5′-end-labeled Rz-12, its molecular stability in cells was investigated. RNA samples extracted from transfected cells were analyzed on PAGE gels (Fig. 5A). Overexposure of the gels was required to reveal all of the bands, as, when exposed normally, only the bands corresponding to the intact ribozyme and the hydrolysis of the U48 phosphodiester bond were detected. Overexposure of the gels confirmed that the banding patterns caused by nuclease degradation in vivo were similar to those obtained in vitro (i.e., in the presence of a protein extract). The only difference in vivo compared to in vitro was the addition of bands corresponding to the hydrolysis of the phosphodiester bonds of the L4 loop (i.e., positions 37, 38, and 39). Because the time considered as zero is, in fact, after trypsination, it is not surprising that a trace amount of ribozyme fragments is observed at the beginning. *Delta* ribozyme appears to be exceptionally stable in this experiment. Various versions of *delta* ribozyme, including the mutants U48A and Rz-12ΔP2, as well as both the hammerhead ribozyme and the $GGG(CU)_{27}$ species, were tested under the same conditions. In all cases, no significant differences, in terms of the identity of the phosphodiester bonds hydrolyzed, was noted between the in vivo and the in vitro experiments.

However, the situation differed significantly with respect to the decay rate constant (Fig. 5B). Rz-12 and mutant U48A have decay curves that are almost identical and do not include a fast decay portion. It seems that these ribozymes have an outstanding stability, and exhibit only a slow decay. After 48 h, the fractions of intact Rz-12 and the U48A mutant remaining were 80% and 85%, respectively. We estimated the $t_{1/2}$ to be over 120 h (see Table 1). Under the same conditions, the hammerhead ribozyme described previously shows a decay that followed a biphasic curve with fast and slow portions characterized by $t_{1/2}$ values of 12 h and 45 h,

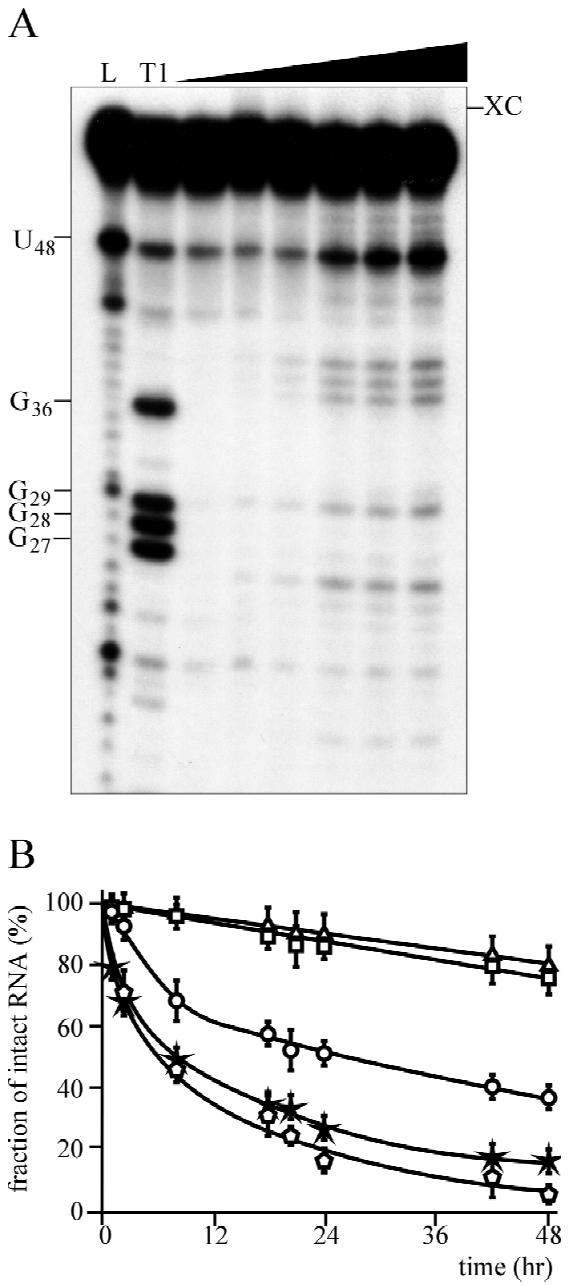

FIGURE 5. In vivo stability of various RNA species. **A:** Autoradiogram of a denaturing 10% PAGE gel of the total RNA recovered from 5′-end-labeled Rz-12 transfected HepG2 cells at various times after transfection. The autoradiogram is overexposed so as to show all bands. The first and second lanes are ladders formed by alkaline (L) and ribonuclease T1 (T1) hydrolysis, respectively. Lanes 3 to 8 represent increasing incubation times (0, 2, 4, 20, 24, 48 h). The migrational position of xylene cyanol (XC) is indicated. **B:** Plot of the fraction of intact RNA species as a function of time for U48A (triangles), Rz-12 (squares), hammerhead ribozyme (circles), Rz-12ΔP2 (stars), and GGG$(CU)_{27}$ (pentagons).

respectively (Table 1). These values are just slightly longer than those obtained in vitro. Finally, both the GGG$(CU)_{27}$ species and the Rz-12ΔP2 mutant exhibited fast decays characterized by $t_{1/2}$ values smaller than 10 h, yielding a relatively small proportion of intact RNA molecules after 48 h (i.e., 8% and 16%, respectively). These small fractions of RNA molecules support the notion that *delta* ribozyme has an intrinsic stability.

To support the last conclusion, we repeated the experiments transfecting the cells by electroporation. Unfortunately, only a small proportion of the cells survived the treatment. Half-life times were determined for some RNA species (Table 1). Hammerhead ribozyme gave a biphasic curve with a constant $t_{1/2}$ regardless of the means of transfection. The Rz-12ΔP2 mutant exhibited a fast decay characterized by a $t_{1/2}$ slightly longer than that observed after lipofection, although this difference is probably not significant. More importantly, the *delta* ribozyme showed a slow decay with a slightly smaller $t_{1/2}$ after electroporation (see Table 1). Thus, if the liposome reagents do indeed protect the transfected *delta* ribozyme in the previous experiments, they do so for only the small fraction that remains associated with the reagent. This conclusion is supported by the repetitive observation that, in contrast to lipofection experiments in which all Rz-12 was observed to be intact after a short period, electroporation produces a small fraction (varying from 5–10%) that degraded almost immediately after the electric shock ($<$1 h), with the bulk then undergoing the slow decay (data not shown). It remains unclear whether this phenomenon is associated with means of transfection or is intrinsic to the ribozyme. Preliminary experiments using calcium phosphate transfection suggest that the same stability (i.e., $t_{1/2}$) can be attributed to the different RNA species (data not shown). However, because the rate of cell death was very high in these experiments, the results varied significantly from one experiment to another. In addition, the high concentration of calcium chloride precipitated the *delta* ribozyme. Thus, we concluded that the increased stability of both Rz-12 and the U48A mutant is due to an increase in molecular stability, and not to an increased duration in the vesicles formed by the liposome reagents.

The $t_{1/2}$ value of 120 h for Rz-12 was an extrapolation of the data from cell aliquots harvested at various intervals over a period of 48 h of growth after liposome transfection. To support the observation of the outstanding stability of *delta* ribozyme in cell culture, we performed an experiment in which cell aliquots were removed after each passage (i.e., each 48 h) for a period of 10 days (Fig. 6). Under these conditions, a $t_{1/2}$ of 112 h was determined directly on the decay curve, a value which is in good agreement with the previous estimation of 120 h. After 10 days, 20% of the Rz-12 remained intact. In contrast, Rz-12ΔP2 appears relatively unstable, with only 20% of intact Rz-12ΔP2 being detected after 48 h, slightly less than 5% after 96 h, and only trace amounts after that ($<$1%). These results shows that the P2 stem plays a critical role in molecular integrity of the ribozyme. Furthermore, this

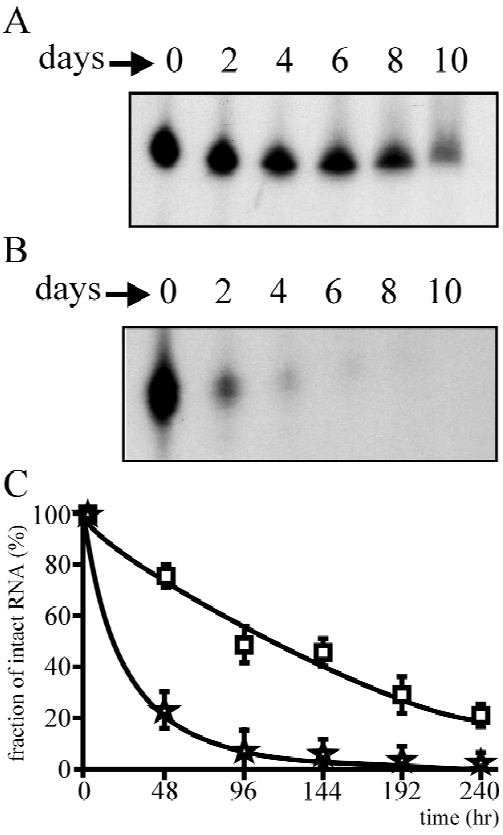

FIGURE 6. Stability of *delta* ribozyme after several cell passages. **A,B:** Autoradiograms of the intact fractions of Rz-12 and Rz-12ΔP2, respectively. Left to right are aliquots retrieved 0, 2, 4, 6, 8, and 10 days after transfection. **C:** Graphical representation of the fraction of intact RNA species as a function of time for Rz-12 (squares) and Rz-12ΔP2 (stars).

is a nice exhibition of the outstanding stability of the *delta* ribozyme.

Localization of the *delta* ribozyme

A plausible explanation for both the large uptake and outstanding stability of *delta* ribozyme is that it is trapped in the cellular membrane. To test this idea, Rz-12 internally labeled with UTP-fluorescein was synthesized, transfected by lipofection as described above, and visualized by confocal laser scanning microscopy (CLSM; Fig. 7). Four hours after the transfection no ribozyme is visible outside of the cellular membrane (Fig. 7A). Using the live cell nucleic acid stain Syto-11 to reveal the nucleus (Fig. 7B), and then superposing it on the previous result (Fig. 7A), it seems that most of the ribozyme is located in the cytoplasm (Fig. 7C). These micrographs show a nonuniform cytosolic (i.e., nonnuclear) localization. We noticed that the intensity of the fluorescent signal varied proportionally with the concentration of ribozyme transfected. When the sensitivity of the detector was increased sufficiently, fluorescence was detected throughout the cytoplasm. Because the confocal microscope provides a tridimensional view, we were able to show that, regardless of the axis of analysis, the fluorescence was always detected, supporting the idea that the ribozyme is distributed throughout the cytoplasm in a nonuniform manner.

When the cells were visualized 30 h after the transfection, results similar to those obtained after 4 h were observed (Fig. 7D–F). This set of figures includes a cell

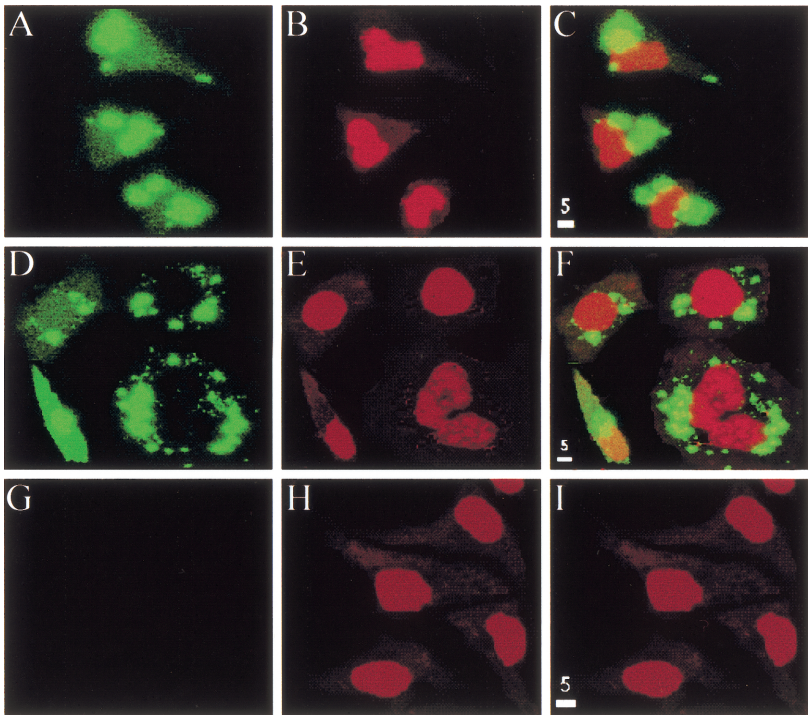

FIGURE 7. Confocal laser scanning microscopy of the intracellular distribution of fluorescein-labeled ribozyme. OST7 cells were transfected with ribozymes and then grown for either 4 h (**A–C**), or 30 h (**D–F**). **G–I:** Cells to which no liposome reagent was added and were grown for 4 h. The cells were either visualized directly, **A**, **D**, and **G**, or after nucleic acid staining with Syto-11 to localize the nucleus **B**, **D**, and **H**. **C**, **F**, and **I** correspond to the superposition of **A**/**B**, **D**/**E**, and **G**/**H**, respectively. The bars represent 5 μm.

in division (bottom right corner), showing that after cell division the ribozyme is equally distributed between the two nascent cells. A close look at Figure 7D, as compared to Figure 7A (i.e., after 30 and 4 h, respectively), reveals that the ribozyme is more diffuse and that a small proportion is found in the nucleus after 30 h, indicating that nuclear exchange had occurred over time. Finally, in the absence of transfection reagent, no ribozyme was detected in the cells (Fig. 7G–I).

The data described above show that *delta* ribozyme is found almost exclusively within the cytoplasm. Similar results were obtained when we repeated the experiments transfecting the cells by electroporation (data not shown). Preferential localization into the cytoplasm was also reported for the hammerhead ribozymes (Prasmickaite et al., 1998); however, it was also shown that hammerhead ribozymes can be equally distributed between the cytoplasm and the nucleus (Bramlage et al., 1999). We investigated whether or not the *delta* ribozymes have a specific subcellular localization by analyzing several transfected cells (data not shown). The ribozymes (i.e., fluorescent signals) were observed to be distributed throughout the cytoplasm of the cells. No specific associations with a particular cellular organelle (e.g., the ribosomes, golgi apparatus, membranes, etc.) were observed. It is not impossible that a small proportion of the ribozymes is associated with intracellular lipofectamine, resulting in a nonuniform distribution. In fact, this hypothesis is supported by the observation that, after 30 h, the ribozyme appeared to be more diffuse, that is the aggregates have divided over time. However, some aggregates were also observed by CLSM after electroporation, suggesting that this association is not only due to the presence of the lipofectamine (data not shown). This observation supports the idea that the liposome reagents are not responsible for the outstanding stability of the *delta* ribozyme. Moreover, ribozymes associated with lipofection reagents would not necessary be inactive. For example, plasmid DNA and RNA delivered by cationic complexes have been shown to be accessible to and functional in both the transcription and translation machinery (Felgner et al., 1987; Malone et al., 1989; Gao & Huang, 1993); and, synthetic hammerhead ribozymes have been used to inhibit luciferase expression (Bramlage et al., 1999).

DISCUSSION

This work shows that natural selection has made *delta* ribozyme ideally suited to the human cell environment, as illustrated by its outstanding stability in these cells. Whereas we find the hammerhead ribozyme to possess both fast and slow decays with estimated $t_{1/2}$ of 11–12 h and 45–49 h, respectively, in agreement with previous reports (Sioud et al., 1994; Gagnon & Rossi, 2000), *delta* ribozyme shows only a slow hydrolysis characterized by a $t_{1/2}$ of over 100 h. This is a significant difference between these ribozymes, meaning that 12 h after transfection only 3% of *delta* ribozymes are hydrolyzed as compared to 40% of the hammerhead species. This outstanding stability appears to be a molecular stability, and not due simply to an increased time spent in the vesicles formed by the liposome reagent. At the very least, if a small portion of the ribozyme molecules remains protected by the cationic liposomes, this might be considered as an important advantage of liposomes as a means for ribozyme delivery because it would have the effect of forming a reservoir that slowly releases soluble molecules. In contrast, when incubated in vitro in the presence of protein extracts isolated from various cell lines, *delta* ribozyme was found to be only a few times more stable than the hammerhead ribozyme. Although the in vitro conditions are significantly different from those found in vivo (e.g., no compartments, different pH), and the nucleases are normally sequestered and activated during preparation of the extract, the magnitude of the reduction of the stability of *delta* ribozyme observed in vitro is surprising.

Presumably, the in vivo stability of the *delta* ribozyme is the result of its evolution as part of the hepatitis *delta* virus RNA within an animal cell, specifically the human hepatocyte. This intrinsic property is reflected by its highly ordered catalytic center, as revealed by the crystal structure, and a number of unusual properties of the *cis*-acting *delta* ribozyme as compared to other self-cleaving RNA motifs (Ferré-D'Amaré et al., 1998; Doherty & Doudna, 2000). For example, it is extremely stable, with an optimal reaction temperature of about 65 °C, and retains activity at temperatures as high as 80 °C and in buffer containing 5 M urea or 18 M formamide. Also, unlike the hammerhead ribozyme, the *delta* ribozyme does not appear able to access alternative *folding* pathways, an observation that, at least in part, could be due to the comparatively limited flexibility of its tightly packed, pseudoknotted tertiary structure (Doherty & Doudna, 2000).

Analysis of the structure of both the original and mutant *delta* ribozymes, and of the regions most susceptible to hydrolysis by the host nuclease, may reveal some clues as to the basis of outstanding stability. The catalytic center is surrounded by two helices, the P2 and P4 stems. The higher vulnerability of the Rz-12ΔP2 indicated that the P2 stem is crucial for the ribozyme's stability, and it seems reasonable to suggest a similar function for the P4 stem. The hydrolysis patterns of the Rz-12ΔP2 mutant, and of the hammerhead ribozyme, suggest that the presence of the single-stranded regions at both the 5′ and 3′ extremities of an uncapped RNA species constitutes a serious drawback in terms of stability. In *delta* ribozyme, both the 5′ and 3′ ends are located within the P2 stem, which appears to be sufficient to greatly stabilize the molecule. Furthermore, the stems forming the *delta* ribozyme sec-

ondary structure appear to be too short to be hydrolyzed by double-strand-specific ribonucleases. The longest stems in this version of the *delta* ribozyme are P2 and P4, which are composed of 6 and 7 bp, respectively. All double-stranded ribonucleases known to date require at least 12 bp as minimal substrate (i.e., a complete helix turn; Nicholson, 1999). Although the single-stranded regions of the catalytic center of *delta* ribozyme are highly ordered, forming a compact pocket, hydrolysis of some phosphodiester bonds was observed. Our data indicates that the hydrolysis appears to be due to the action of single-strand-specific endoribonucleases, more precisely those that recognize the phosphodiester bonds between either pyrimidines or uridine–adenine, which are believed to be predominant in human cells (Sorrentino, 1998). We observed hydrolysis at phosphodiester bonds composed of cytosine–uridine (U_{10}, U_{13}, and U_{48}), uridine–cytosine (C_{14}), and uridine–adenine (A_{49}) linkages. Thus, with the exception of the uridine–cytosine (C_{11}) and cytosine–cytosine (C_{12}), all phosphodiester bonds between these types of nucleotides within the catalytic center were hydrolyzed. Therefore, a systematic mutagenic attack of the tertiary structure was not justified; rather a more rational and focused approach was appropriate. The U_{10} is crucial to the catalytic activity of the ribozyme and therefore cannot be mutated. Direct mutagenesis of the four other nucleotides (positions 13, 14, 48, and 49) failed to generate a more stable ribozyme that retained the same catalytic potential. Rz-12, which was based largely on the wild-type sequence, remains the best tested ribozyme in terms of both catalysis and stability. This is in good agreement with the observation that within the natural HDV variants sequenced to date, only a small number of mutations were observed within the bases forming the catalytic center of these self-cleaving RNA motifs (J.P. Perreault, unpubl. data). Evolution has not only produced a global architecture for the *delta cis*-acting ribozyme, but also a precise nucleotide sequence.

The outstanding stability of the *delta* ribozyme appears to be a result of its compact tertiary structure, which includes a catalytic center surrounded by two helices. We cannot rule out the possibility that a cellular protein interacts with *delta* ribozyme, protecting it against ribonucleases. However, preliminary crosslinking experiments failed to detect a ribozyme/protein complex (data not shown). Consequently, we suggest that the outstanding stability of *delta* ribozyme is the result of its adaptation to the human protein environment. It is not protected like the products of RNA polymerases I and III by proteins, nor by amino acids like tRNA. Moreover, it has nothing in common with the products of RNA polymerase II (mRNA). *Delta* ribozymes do not possess the usual features of mRNA (i.e., 5′-cap, poly(A) tail, inside motif) that are recognized by the proteins involved in their degradation (for a review, see Guhaniyogi & Brewer, 2001).

One of the factors limiting the development of hammerhead ribozyme as a gene-inactivation tool is its stability, or lack thereof. Sioud et al. (1994) reported that transfected hammerhead ribozymes followed a biphasic decay with both fast and slow rate constants. It was suggested that two different populations of ribozymes were present; one that was rapidly degraded by the host nucleases (i.e., $t_{1/2}$ of 1.7–3.0 h), and a second that was folded in a such manner that it was resistant to degradation. Our results with the hammerhead ribozyme are virtually identical. In contrast, the *delta* ribozyme appears to adopt a single conformation that is resistant to both the murine and human nucleases (i.e., OST7 and HepG2 cells).

In addition to this exceptional stability, and its natural ability to function in the presence of human proteins, *delta* ribozyme has several other distinctive features that, unique among the small ribozymes ($<$100 nt), may constitute advantages for its development as a therapeutic tool. For example, it has the ability to function efficiently at a relatively low concentration of either magnesium or calcium ($\sim$1 mM, i.e., human-like physiological conditions). Also, it has the ability to effectively carry out general acid–base catalysis (Nakano et al., 2000). The extrapolated rate constant for the chemical step in the *delta* ribozyme reaction may approach that for cleavage by RNase A (Nakano et al., 2000). Therefore, the next critical research step with this ribozyme was to deliver a proof-of-concept that it functions in vivo to cleave an RNA in *trans*. Evidence supporting the cleavage of a BCR-ABL chimeric mRNA, which causes a chronic myelogenous leukemia, by *delta* ribozyme was recently reported (Kato et al., 2001). This report demonstrated that a *delta* ribozyme, whose activity in vitro was almost three orders of magnitude lower than that of a hammerhead ribozyme, still exhibited similar activity in cells. This higher level of activity in vivo of the *delta* ribozyme, as compared to that observed in vitro, could be partly attributed to its outstanding stability. Additional evidence comes from a recent experiment showing that Rz-12 significantly reduces the levels of both the HDAg mRNA and the corresponding protein in cell culture (D. Lévesque & J.P. Perreault, unpubl. data), thereby confirming the potential of *delta* ribozyme. The natural adaptability of this ribozyme to the human cell may constitute a breakthrough for the development of a gene-inactivation system based on a nucleic acid. At the very least, it should reestablish the possibility of using either a plasmid or a viral vector to introduce a ribozyme gene from which a stable ribozyme would be produced intracellularly.

MATERIALS AND METHODS

Plasmids encoding *delta* ribozymes

The construction of plasmids carrying *trans*- and *cis*-acting ribozymes (i.e., Rz-1, Rz-6, Rz-11, Rz-12, Rz-12C47A, and a

cis-acting version) has been described previously (Roy et al., 1999; Ananvoranich & Perreault, 2000). The Rz-12 mutants were prepared as follows. Two complementary oligonucleotides (500 pmol each) corresponding to the T7 RNA promoter and the Rz-12 gene with the four positions of interest (i.e., 13, 14, 48, and 49) randomized (50% of each of the desired bases; see Fig. 4) were annealed together in a final volume of 20 μL containing 10 mM Tris-HCl, pH 7.5, 10 mM $MgCl_2$, and 50 mM KCl. This annealing generated a product with extremities compatible with those generated by *Pst*I and *Hin*dIII digestion; hence, the annealed products could be directly ligated to predigested pUC19 vector. The 15 Rz-12 mutants were selected on the basis of DNA sequencing data.

RNA synthesis

Substrate molecules (11 nt) were prepared by annealing two pairs of complementary and overlapping oligonucleotides in a final volume of 20 μL containing 10 mM Tris-HCl, pH 7.5, 10 mM $MgCl_2$, and 50 mM KCl by incubating at 85 °C for 2 min and then allowing the mixture to slowly cool to 37 °C. Using the resulting partial duplex as template (500 pmol), in vitro transcription reactions were carried out in a final volume of 50 μL containing 27 U of RNAGuard (Amersham Pharmacia Biotech), 4 mM of each NTP (ATP, GTP, CTP, and UTP), 80 mM HEPES-KOH, pH 7.5, 24 mM $MgCl_2$, 2 mM spermidine, 40 mM DTT, 0.01 U yeast pyrophosphatase, and 25 μg purified T7 RNA polymerase at 37 °C for 4 h, as described previously (Ananvoranich & Perreault, 1998). The samples were then DNase (RNase-free, Promega) treated, and the transcripts purified on denaturing (7 M urea) 20% polyacrylamide gels using 50 mM Tris-borate, pH 8.3/1 mM EDTA solution as running buffer. The reaction products were visualized by ultraviolet shadowing over a fluorescent thin-layer chromatography plate, and the bands corresponding to the correct sizes cut out. Transcripts were eluted from these gel slices by incubating overnight at 4 °C in a 0.1% SDS/0.5 M ammonium acetate solution. They were then precipitated by adding 0.1 vol of 3 M sodium acetate, pH 5.2, and 2.2 vol of ethanol, and the resulting pellet washed with 70% ethanol and dried. After dissolving in nanopure water, the purified transcripts were quantified by spectrophotometry at 260 nm. The same approach using long DNA oligonucleotides was used to prepare the *trans*-acting hammerhead structure derived from the peach latent mosaic viroid strand of minus polarity, the $GGG(CU)_{27}$, and the Rz-12ΔP2 mutant (see Fig. 3). The various versions of *delta* ribozymes were synthesized using *Sma*I-linearized plasmid (10 μg), which had been purified by both phenol and chloroform extractions, and precipitated for further use as template in transcription reactions as described above. The fluorescein-labeled ribozymes were synthesized using the same transcription protocol except that the fluorescein RNA labeling 10× mix containing 10 mM ATP, 10 mM CTP, 10 mM GTP, 6.5 mM UTP, and 3.5 mM fluorescein-12-UTP (Roche Diagnostic) was used.

5′-end labeling of RNA

Purified RNA species (10 pmol) were dephosphorylated in a final volume of 20 μL containing 200 mM Tris-HCl, pH 8.0, 10 U of RNAGuard, and 0.2 U of calf intestinal alkaline phosphatase (Amersham Pharmacia Biotech) at 37 °C for 30 min, and were then purified by extracting twice with an equal volume of phenol/chloroform (1:1) and ethanol precipitating. Dephosphorylated transcripts (1 pmol) were 5′-end labeled in a final volume of 10 μL containing 1.6 pmol [γ-^{32}P]ATP (New England Nuclear), and 3 U of T4 polynucleotide kinase as recommended by the manufacturer (Amersham Pharmacia Biotech). Excess [γ-^{32}P]ATP was removed by passage through a G-50 Sephadex (Amersham Pharmacia Biotech) spin column. The concentration of the labeled transcripts was adjusted to 0.01 pmol/μL by the addition of water.

In vitro cleavage assays and kinetic analyses

Cleavage assays were performed at 37 °C under single-turnover conditions with trace amounts of the 5′-end-labeled small substrates (<1 nM) and an excess of ribozyme (200 nM) in a final volume of 20 μL containing 50 mM Tris-HCl, pH 7.5, and 10 mM $MgCl_2$. The mixtures were heated at 95 °C for 2 min, snap-cooled on ice for 1 min, and then preincubated for 5 min at 37 °C prior to the addition of the magnesium that initiates the reaction. Aliquots (2 μL) were periodically removed, added to stop solution (5 μL, 97% formamide, 10 mM EDTA, 0.25% bromophenol blue, and 0.25% of xylene cyanol), quickly frozen, and subsequently analyzed by electrophoresis through 20% denaturing PAGE gels followed by autoradiography. Substrate and product bands were quantified with a PhosphorImager (Molecular Dynamics). Kinetic parameters were determined by means of nonlinear curve-fitting based on pseudo-first-order analysis. The fractions of substrate cleaved were determined, and the rate constants (k_{obs}) and maximal cleavage percentage obtained by fitting the data to the equation $A_t = A_0(1 - e^{-kt})$, where A_t is the percentage of cleavage at time t, A_0 is the maximum percentage of cleavage (or the end point of cleavage), and k is the rate constant (k_{obs}). Each rate constant was calculated from at least two independent measurements. Kinetic analyses were performed under single-turnover conditions as described previously (Ananvoranich & Perreault, 1998). Various concentrations of unlabeled ribozymes (5–400 nM) were mixed in a final volume of 18 μL, and the reactions were performed and analyzed as described. The fractions of substrate cleaved were determined, and the rate of cleavage (k_{obs}) was obtained from at least two independent measurements. The k_{obs} were plotted as a function of ribozyme concentration for the determination of the kinetic parameters [apparent catalytic rate constant (k_2) and apparent Michaelis-Menten constant (K'_M)].

In vitro stability of various RNA species

The protein extracts were prepared from a single 100-mm petri-dish culture of either HepG2, OST7 (Elroy-Stein & Moss, 1990), or HEK 293 cells. In all cases, the cells were grown at 37 °C to 80% confluence prior to harvesting, and were then washed with PBS buffer (137 mM NaCl, 2.7 mM KCl, 10.1 mM Na_2HPO_4, 1.8 mM KH_2PO_4, pH 7.4). The washed cells were treated with trypsin, centrifuged at 13,000 rpm for 1 min, resuspended in 4 mL of PBS buffer, and subjected to three freeze/thaw cycles. Centrifugation for 5 min at 13,000 rpm in

an Eppendorf centrifuge gave a supernatant that constituted the protein extract used for the various assays. The protein concentration of this mixture was determined using the Bradford method. Protein extracts were diluted in 250 mM Tris-HCl, pH 7.5/50 mM $MgCl_2$ solution so as to have a protein concentration of 0.0625 μg/μL. Prior to incubation, the RNA species (500 ng of ^{32}P-5′-end-labeled RNA) were resuspended in a final volume of 32 μL containing 10 mM Tris-HCl, pH 7.5, heat-denatured at 95 °C for 2 min, snap-cooled on ice for 1 min, and preincubated at 37 °C for 5 min. Protein extract (500 ng) was then added to the mixture containing the radiolabeled ribozyme. When required, the amount of protein extract was varied, but in all cases, the chemical components were adjusted so as to ensure a final volume of 40 μL. Aliquots (1 or 2 μL) were recovered at various time points and immediately mixed with stop solution and quickly electrophoresed on denaturing 10% or 20% PAGE gels. The resulting dried gels were revealed by autoradiography or PhosphorImager (Molecular Dynamics). The fraction of intact RNA species remaining was determined as a percentage of all bands observed in a gel lane. These percentages were plotted as a function of time, and $t_{1/2}$ were estimated as described in the Results section, taking into account whether the degradation was monophasic or biphasic (see also Sioud et al., 1994). The results of at least two independent experiments were combined for each RNA species analyzed.

Transfection and in vivo stability

HepG2, OST7, or HEK 293 cells, grown at 37 °C to 80% confluence in 100-mm petri dishes, were transfected with radioactive ribozymes, or other RNA species, using either Lipofectamine (Gibco-BRL) or Effectene (Qiagen) as recommended by the manufacturer. After transfection, the cells were grown for 4 h in MEM media (Gibco-BRL) without serum. The cells were then trypsinized, harvested, and washed twice with PBS buffer. The cell pellet was resuspended in MEM media containing serum (2 mL per sample), and divided into several equal samples that were grown for different intervals of time. At the appropriate time points, the cells were recovered, washed at least three times with PBS buffer, and the RNA extracted using Trizol as recommended by the manufacturer (Gibco-BRL). Total RNA was always resuspended in 40 μL of nanopure water. Uniform RNA recovery and integrity was verified by OD_{260} reading and agarose gel analysis, respectively, of each aliquot. Total RNA samples (15 μL) were mixed with 8 μL of stop solution and analyzed on denaturing 10% or 20% PAGE gels. The dried gels were revealed by autoradiography or PhosphorImager, and were quantified as described previously. Some transfections were also performed by electroporation. In that case, OST7 cells grown at 37 °C to 80% confluence in 100-mm petri dishes were transferred to electroporation cuvettes with a 4-mm gap (BioRad). The cells were then electroporated at 210 V (960 μF) using a Gene Pulser I electroporator system (BioRad).

Confocal laser scanning microscopy

Following the transfection of fluorescein-labeled ribozyme into either HepG2 or OST7 cells, aliquots were recovered after 4 and 30 h as described above. The recovered cells were washed with phosphate buffer, and the unfixed cells examined with a Molecular Dynamics Multi Probe 2001 confocal argon scanning microscope (CLSM) equipped with a Nikon Diaphot epifluorescence inverted microscope and a 60× (1.4 NA) Nikon oil Plan achromat objective as described previously (Bkaily et al., 1999). The 488-nm argon laser line (99.0 mV) was directed to the sample via a 510 nm primary dichroic filter and attenuated with a 3% neutral density filter to reduce photobleaching. Pinhole line intensity, photometric gain, PMT setting, and filter attenuation were kept constant throughout all experimental procedures. At the end of each experiment, the nucleus was stained with 100 nM of live cell nucleic acid stain Syto-11 (Molecular Probes). Pixel intensities in individual cells were read from the images after background substraction using Image 2 software. Further image processing was performed with Imaris software on a Silicon graphics computer system. Confocal stacks of green and red fluorescence were visualized in section view mode.

ACKNOWLEDGMENTS

We thank Dr. Ghassan Bkaily for providing access to and technical advice on the use of the confocal microscope. This work was sponsored by a grant from both the Canadian Institute of Health Research (CIHR) and Health Canada to J.P.P., who is also the recipient of a CIHR investigator award.

Received July 9, 2001; returned for revision September 1, 2001; revised manuscript received January 23, 2002

REFERENCES

Ananvoranich S, Perreault JP. 1998. Substrate specificity of δ ribozyme cleavage. *J Biol Chem 273*:13182–13188.

Ananvoranich S, Perreault JP. 2000. The kinetics and magnesium requirements for the folding of antigenomic δ ribozymes. *Biochem Biophys Res Comm 270*:600–607.

Beaudry D, Bussière F, Lareau F, Lessard C, Perreault JP. 1995. The RNA of both polarities of the peach latent mosaic viroid self-cleaves in vitro solely by single hammerhead structures. *Nucleic Acids Res 23*:745–752.

Been MD, Wickham GS. 1997. Self-cleaving ribozymes of hepatitis *delta* virus RNA. *Eur J Biochem 247*:741–753.

Bkaily G, Jacques D, Pothier P. 1999 Use of confocal microscopy to investigate cell structure and function. *Methods Enzymol 307*:119–135.

Bramlage B, Alefelder S, Marschall P, Eckstein F. 1999. Inhibition of luciferase expression by synthetic hammerhead ribozymes and their cellular uptake. *Nucleic Acids Res 27*:3159–3167.

Chowrira BH, Pavco PA, McSwiggen JA. 1994. In vitro and in vivo comparison of hammerhead, hairpin, and hepatitis *delta* virus self-processing ribozyme cassettes. *J Biol Chem 269*:25856–25864.

Doherty EA, Doudna JA. 2000. Ribozyme structure and mechanism. *Annu Rev Biochem 69*:597–615.

Elroy-Stein O, Moss B. 1990. Cytoplasmic expression system based on constitutive synthesis of bacteriophage T7 RNA polymerase in mammalian cells. *Proc Natl Acad Sci USA 87*:6743–6747.

Felgner PL, Gadek TR, Holm M, Roman R, Chan HW, Wenz M, Northrop JP, Ringold GM, Danielsen M. 1987. Lipofection: highly efficient lipid-mediated DNA-transfection procedure. *Proc Natl Acad Sci USA 84*:7413–7417.

Ferré-D'Amaré AR, Zhou K, Doudna JA. 1998. Crystal structure of a hepatitis *delta* virus ribozyme. *Nature 395*:567–574.

Gagnon L, Rossi JJ. 2000. Downregulation of the CCR5 β-chemokine receptor and inhibition of HIV-1 infection by stable VA1-ribozyme

chimeric transcripts. *Antisense Nucleic Acids Drug Dev 10*:251–261.
Gao X, Huang L. 1993. Cytoplasmic expression of a reporter gene by co-delivery of T7 RNA polymerase and T7 promoter sequence with cationic liposomes. *Nucleic Acids Res 21*:2867–2872.
Guhaniyogi J, Brewer G. 2001. Regulation of mRNA stability in mammalian cells. *Gene 265*:11–23.
Kariko K, Megyeri K, Xiao Q, Barnathan ES. 1994. Lipofection-aided cell delivery of ribozyme targeted to human urokinase receptor mRNA. *FEBS Lett 352*:41–44.
Kato Y, Kuwabara T, Warashina M, Toda H, Taira K. 2001. Relationships between the activities in vitro and in vivo of various kinds of ribozyme and their intracellular localization in mammalian cells. *J Biol Chem 276*:15378–15385.
Lafontaine DA, Mercure S, Perreault JP. 1997. Update of the viroid and viroid-like sequence database: Addition of a hepatitis *delta* virus RNA section. *Nucleic Acids Res 25*:123–125.
Malone RW, Felgner PL, Verma IM. 1989. Cationic liposome-mediated RNA transfection. *Proc Natl Acad Sci USA 86*:6077–6081.
Mercure S, Lafontaine DA, Ananvoranich S, Perreault JP. 1998. Kinetic analysis of δ ribozyme cleavage. *Biochemistry 37*:16975–16982.
Nakano SI, Chadalavada DM, Bevilacqua PC. 2000. General acid-base catalysis in the mechanism of a hepatitis *delta* virus ribozyme. *Science 287*:1493–1497.
Nicholson AW. 1999. Function mechanism and regulation of bacterial ribonucleases. *FEMS Microbiol Rev 23*:371–390.
Nishikawa F, Nishikawa S. 2000. Requirement for canonical base pairing in the short pseudoknot structure of genomic hepatitis *delta* virus ribozyme. *Nucleic Acids Res 28*:925–931.
Pattnaik AK, Ball LA, LeGrone AW, Wertz GW. 1992. Infectious defective interfering particles of VSV from transcripts of a cDNA clone. *Cell 69*:1011–1020.
Prasmickaite L, Hogset A, Maelandsmo G, Berg K, Goodchild J, Perkins T, Fodstad O, Hovig E. 1998. Intracellular metabolism of a 2′-*O*-methyl-stabilized ribozyme after uptake by DOTAP transfection or as free ribozyme. A study by capillary electrophoresis. *Nucleic Acids Res 26*:4241–4248.
Rossi J. 2000. Ribozyme therapy for HIV infection. *Adv Drug Deliv Rev 44*:71–78.
Roy G, Ananvoranich S, Perreault JP. 1999. *Delta* ribozyme has the ability to cleave in *trans* an mRNA. *Nucleic Acids Res 27*:942–948.
Sioud M, Opstad A, Zhao JQ, Levitz R, Benham C, Drlica K. 1994. In vivo decay kinetic parameters of hammerhead ribozymes. *Nucleic Acids Res 22*:5571–5575.
Sorrentino S. 1998. Human extracellular ribonucleases: Multiplicity, molecular diversity and catalytic properties of the major RNase types. *Cell Mol Life Sci 54*:785–794.
Verma S, Eckstein F. 1998. Modified oligonucleotides—Synthesis and strategy for users. *Annu Rev Biochem 67*:99–134.
Wadkins TS, Perrotta AT, Ferré-D'Amaré AR, Doudna JA, Been MD. 1999. A nested double pseudoknot is required for self-cleavage activity of both the genomic and antigenomic hepatitis *delta* virus ribozymes. *RNA 5*:720–727.